# Direct Detection and Measurement of Electron Relays in a Multicentered Enzyme: Voltammetry of Electrode-Surface Films of *E. coli* Fumarate Reductase, an Iron−Sulfur Flavoprotein

**Hendrik A. Heering,[†] Joel H. Weiner,[‡] and Fraser A. Armstrong*[,†]**

*Contribution from the Inorganic Chemistry Laboratory, Oxford University, South Parks Road, Oxford OX1 3QR, England, and Department of Biochemistry, University of Alberta, Edmonton, Alberta, Canada T6G 2H7*

*Received July 11, 1997*[⊗]

**Abstract:** Intramolecular electron relays operating in a multicentered enzyme are revealed by protein film voltammetry. The membrane-extrinsic catalytic domain of *E. coli* fumarate reductase (FrdAB) adsorbs to electroactive monolayer coverage at a rotating pyrolytic graphite edge electrode, giving characteristic voltammetric signals that are resolved and assigned to redox-active sites. At pH 7.3 (2 °C), signals attributable to Centers 1 ([2Fe-2S]) and 3 ([3Fe-4S]) and FAD are enveloped together around −50 mV, while Center 2 ([4Fe-4S]) appears as a weaker signal at −305 mV. At pH 9.5, similar voltammetry is observed, the main difference being that the FAD component shifts to the negative edge of the envelope. The prominence of the two-electron FAD signal enables active-site redox transformations to be tracked and examined over a range of conditions. Scans at rates up to 20 V $s^{-1}$ in the absence of fumarate show that electrons are relayed to the FAD, most obviously by Centers 1 and 3. Upon adding fumarate, the signals undergo transformations as specific centers engage in catalytic electron transport. A sigmoidal wave originating in the FAD envelope region is joined by a second wave close to the potential of Center 2. This is particularly evident under conditions optimizing enzyme catalytic control (as opposed to mass-transport control), i.e. high fumarate levels, high rotation rate, and pH 9.0 at which the enzyme is less active than at pH 7.0. Intramolecular electron transport is partitioned between different relay systems depending on catalytic demand and proficiency of the FAD as electron acceptor. At high pH, the less favorable driving force for electron transfer from Centers 1 and 3 places a greater burden on Center 2. Catalytic voltammograms show hysteresis in the presence of oxalacetate, an inhibitor binding preferentially to oxidized FAD. Reductive activation is slow but accelerates sharply below the potential of Center 2, showing that this cluster is much more effective than the others in reducing the inhibitor-bound active site. The results demonstrate how voltammetry can be used to quantify intramolecular electron transfer among multiple sites in complex enzymes.

## Introduction

Electron-transport enzymes typically contain redox-active metal centers in addition to the catalytic site(s) at which small substrates are intimately bound and transformed.[1] These supernumerary centers may have several functions; for example, they may service the supply of electrons to and from the active site by acting as "relay stations" or storage sites, while they may also act as regulators by linking activity or structure to redox state or binding of effectors. Biological "wiring" of enzymes utilizes one or more "relay stations" organized to optimize overall efficiency.[2] (The term *relay* refers to a sequence of "real" stations between which electrons move, as opposed to *pathway* which refers to the intervening "virtual" medium through which electrons tunnel.[3]) Ideally, fast electron transfer depends on minimum through-bond or through-space distances between relay stations,[2,3] which, it is tacitly assumed, should be organized in the direction of increasing reduction potential.

We are utilizing the voltammetry of proteins that are (ideally) innocuously adsorbed on an electrode in an electroactive state to study the properties and functions of redox-active centers.[4] Our efforts in this area—protein film voltammetry—have so far ranged from studies of labile, air-sensitive Fe−S clusters[5] to the high-potential (Fe(IV)) chemistry of cytochrome *c* peroxidase.[6] We have used protein-film voltammetry also to investigate catalytic electron transport in complex multicentered

[†] Oxford University.

[‡] University of Alberta.

[⊗] Abstract published in *Advance ACS Abstracts,* November 15, 1997.

(1) Structures of some important multicentered electron-transport enzymes have been determined. See, for example: Messerschmidt, A.; Lücke, H.; Hüber, R. *J. Mol. Biol.* **1993**, *230*, 997−1014. Kim, J. S.; Rees, D. C. *Nature* **1992**, *360*, 553−560. Georgaiadis, M. M.; Komiya, H.; Chakrabarti, P.; Woo, D.; Kornuc, J. J.; Rees, D. C. *Science* **1992**, *257*, 1653−1659. Volbeda, A.; Charon, M-H.; Piras, C.; Hatchikian, E. C.; Frey, M.; Fontecilla-Camps, J. C. *Nature* **1995**, *373*, 580−587. Iwata, I.; Ostermeier, C.; Ludwig, B.; Michel, H. *Nature* **1995**, *376*, 660−669. Tsukihara, T.; Aoyama, H.; Yamashita, E.; Tomikazi, T.; Yamaguchi, H.; Shinzawa-Itoh, K.; Nakashima, R.; Yaono, R.; Yoshikawa, S. *Science* **1995**, *269*, 1069−1074. Deisenhofer, J.; Epp, O.; Sinning, I.; Michel, H. *J. Mol. Biol.* **1995**, *246*, 429−457.

(2) Christensen, H. E. M.; Coutinho, I.; Conrad, L. S.; Hammerstad-Pedersen, J. M.; Iversen, G.; Jensen, M. H.; Karlsson, J. J.; Ulstrup, J.; Xavier, A. V. *J. Photochem. Photobiol. A: Chem.* **1994**, *82*,103−115. For an account of artificial "wiring" of enzymes, see also: Heller, A. *Acc. Chem. Res.* **1990**, *23*, 128−134.

(3) Moser, C. C.; Keske, J. M.; Warncke, K.; Farid, R. S.; Dutton, P. L. *Nature* **1992**, *355*, 796−802. Beratan, D. N.; Betts, J. N.; Onuchic, J. N. *Science* **1991**, *252*, 1285−1288. See also, articles in the following: Bendall, D. S., Ed. *Protein Electron Transfer*; Bios Scientific Publishers: Oxford, 1996.

(4) Armstrong, F. A.; Butt, J. N.; Sucheta, A. *Methods Enzymol.* **1993**, *227*, 479−500. Armstrong, F. A. In Bioelectrochemistry: Principles and Practice; Lenaz, G.; Milazzo, G., Eds.; Bioelectrochemistry of Macromolecules, Vol. 5; Birkhauser Verlag: Basel 1997. Armstrong, F. A.; Heering, H. A.; Hirst, J. *Chem. Soc. Rev.* **1997**, *26*, 169−179.

S0002-7863(97)02324-X CCC: $14.00 

enzymes, in particular succinate dehydrogenase[7−9] and fumarate reductase.[10] The technique allows interactive examination of complex systems, enabling (for enzymes) the simultaneous observation of steady-state catalysis and active-site redox transformations as precise functions of potential as well as the more familiar kinetic (time) domain.[8,9] Importantly, ET is induced and measured in either direction, over a wide kinetic range, and under controlled, tunable conditions of driving force. Confinement of the protein as a mono-submonolayer enables miniscule sample quantities to be studied and alleviates the limitations due to complex and sluggish diffusion of the macromolecule to and from the electrode surface.[4] The sharp and finite voltammetric response of surface-confined species enhances resolution and facilitates detection of redox centers and determination of their stoichiometries.[4] Rates of interfacial electron transfer (i.e., between the electrode and the redox sites) depend largely on distance,[11] but in favorable cases will far exceed the turnover rate of the enzyme. With such facile electron exchange, and with efficient mass transport of substrates, the observed catalytic wave form is limited by (and thus reports on) intrinsic properties of the enzyme, including the organization of intramolecular relays.[10]

This paper describes a study of intramolecular ET relays in a very electroactive enzyme, fumarate reductase (Frd, or menaquinol:fumarate oxidoreductase: EC 1.3.99.1) from *E. coli*. This enzyme, like its mitochondrial counterpart succinate: ubiquinone oxidoreductase (complex II), exists *in vivo* as a membrane-bound complex linking the two-electron interconversion of fumarate and succinate to the quinone pool[12]

$$\text{fumarate} + QH_2 \rightleftarrows \text{succinate} + Q \qquad (1)$$

Fumarate reductase catalyzes the final stage in anaerobic respiration with fumarate as the terminal electron acceptor. The FrdAB complex is located in the cytoplasmic membrane and consists of four subunits.[12,13] Two subunits (FrdC and FrdD) form the membrane anchor domain and contain the binding sites for menaquinol.[14,15] The other two subunits (FrdA and FrdB) are tightly interassociated and form the membrane-extrinsic soluble domain: FrdA (66 kDa) contains the substrate binding site and a covalently bound 8α-[*N*(3)-histidyl] FAD, while FrdB (27 kDa) contains three types of iron−sulfur cluster; Center 1 ($[2Fe\text{-}2S]^{2+/1+}$), Center 2 ($[4Fe\text{-}4S]^{2+/1+}$), and Center 3 ($[3Fe\text{-}4S]^{1+/0}$).[12,13,16,17] Reported equilibrium reduction potentials $E^{0\prime}$ and other relevant data are listed in Table 1.[12,18−26] Values for Centers 1 and 3 and the FAD are appropriate for mediating electron transfer between menaquinone and fumarate, whereas $E^{0\prime}$ for Center 2 is conspicuously negative, posing a question as to its function and physiological role. On the basis of individual items of kinetics and potentiometric information on both FrdAB and Complex II, suggestions range from the idea[27] that Center 2 functions *in parallel* to Centers 1 and 3 (providing a second relay between FAD and ubiquinone) to one in which Center 2 acts *in series*,[28] its apparent (equilibrium) potential lowered by interaction with the other centers. It has also been proposed that Center 2 preserves structural integrity and membrane-binding functions[16] although a redox role was subsequently reaffirmed by studies showing a lower growth rate and activity for mutants in which Center 2 has a more negative reduction potential.[23]

**Table 1.** Reported Reduction Potentials of Fumarate Reductase and References (Conditions Vary)

| | |
|---|---|
| FAD | −48 mV (25 °C) and −30 mV (3 °C) at pH 7;[10] −55 mV[18] |
| Center 1 | −20 mV;[19] −50 mV;[20,21] −79 mV[16,22,23] |
| Center 2 | −285 mV;[20,21] −300 mV;[16,22,23] −311 mV;[10] −320 mV[19] |
| Center 3 | −30 mV;[20] −50 mV;[21] −70 mV[16,19,22,23] |
| menaquinone | −70 mV;[24] −74 mV[24,25] |
| fumarate | +30 mV (pH 7)[26] |

The membrane anchor domain of fumarate reductase is essential for reaction with menaquinone.[14,15] However, a soluble enzyme FrdAB consisting only of the membrane-extrinsic subunits FrdA and FrdB can be prepared which is active in fumarate reduction by benzylviologen.[29,30] It was reported previously[10] that an adsorbed film of FrdAB equivalent to an electroactive monolayer can be immobilized at a pyrolytic graphite edge electrode. The adsorbed enzyme exhibits excel-

(5) Butt, J. N.; Armstrong, F. A.; Breton, J.; George, S. J.; Thomson, A. J.; Hatchikian, E. C. *J. Am. Chem. Soc.* **1991**, *113*, 6663−6670. Butt, J. N.; Sucheta, A.; Armstrong, F. A.; Breton, J.; Thomson, A. J.; Hatchikian, E. C. *J. Am. Chem. Soc.* **1991**, *113*, 8948−8950. Butt, J. N.; Niles, J.; Armstrong, F. A.; Breton, J.; Thomson, A. J. *Nat. Struct. Biol.* **1994**, *1*, 427−433. Breton, J. L.; Duff, J. L. C.; Butt, J. N.; Armstrong, F. A.; George, S. J.; Pétillot, Y.; Forest, E.; Schäfer, G.; Thomson, A. J. *Eur. J. Biochem.* **1995**, *233*, 937−946. Duff, J. L. C.; Breton, J. L. J.; Butt, J. N.; Armstrong, F. A.; Thomson, A. J. *J. Am. Chem. Soc.* **1996**, *118*, 8593−8603. Butt, J. N.; Fawcett, S. E. J.; Breton, J.; Thomson, A. J.; Armstrong, F. A. *J. Am. Chem. Soc.* **1997**, *119*, 9729.

(6) Mondal, M. S.; Fuller, H. A.; Armstrong, F. A. *J. Am. Chem. Soc.* **1996**, *118*, 263−264.

(7) Sucheta, A.; Ackrell, B. A. C.; Cochran, B.; Armstrong, F. A. *Nature* **1992**, *356*, 361−362.

(8) Hirst, J.; Sucheta, A.; Ackrell, B. A. C.; Armstrong, F. A. *J. Am. Chem. Soc.* **1996**, *118*, 5031−5038.

(9) Hirst, J.; Ackrell, B. A. C.; Armstrong, F. A. *J. Am. Chem. Soc.* **1997**, *119*, 7434−7439.

(10) Sucheta, A.; Cammack, R.; Weiner, J.; Armstrong, F. A. *Biochemistry* **1993**, *32*, 5455−5465.

(11) Song; S.; Clark, R. A.; Bowden, E. F.; Tarlov, M. J. *J. Phys. Chem.* **1993**, *97*, 6564−6572. Feng, Z. Q.; Imabayashi, S.; Kakiuchi, T.; Niki, K. *J. Electroanal. Chem.* **1995**, *394*, 149−154. Nahir, T. M.; Bowden, E. F. *J. Electroanal. Chem.* **1996**, *410*, 9−13.

(12) Ackrell, B. A. C.; Johnson, M. K.; Gunsalus, R. P.; Cecchini, G. *Chemistry and Biochemistry of Flavoenzymes*; Müller, F., Ed.; CRC Press: Boca Raton, FL, 1992; Vol. III, pp 230−297. Hederstedt, L.; Ohnishi, T. In *Molecular Mechanisms in Bioenergetics*; Ernster, L., Ed.; Elsevier: New York, 1992, pp 163−198.

(13) Weiner, J.; Dickie, P. *J. Biol. Chem.* **1979**, *254*, 8590−8593. Blaut, M.; Whittaker, K.; Valdovinos, A.; Ackrell, B. A. C.; Gunsalus, R. P.; Cecchini, G. *J. Biol. Chem.* **1989**, *264*, 13599−13604.

(14) Weiner, J. H.; Cammack, R.; Cole, S. T.; Condon, C.; Honore, N.; Lemire, B. D.; Shaw, G. *Proc. Natl. Acad. Sci. U.S.A.* **1986**, *83*, 2056−2060.

(15) Westenberg, D. J.; Gunsalus, R. P.; Ackrell, B. A. C.; Cecchini, G. *J. Biol. Chem.* **1990**, *265*, 19560−19567.

(16) Manodori, A.; Cecchini, G.; Schröder, I.; Gunsalus, R. P.; Werth, M. T.; Johnson, M. K. *Biochemistry* **1992**, *31*, 2703−2712.

(17) van Hellemond, J. J.; Tielens, A. G. M. *Biochem. J.* **1994**, *304*, 321−331.

(18) Ackrell, B. A. C.; Cochran, B.; Cecchini, G. *Arch. Biochem. Biophys.* **1989**, *268*, 26−34.

(19) Cammack, R.; Patil, D. S.; Weiner, J. H. *Biochim. Biophys. Acta* **1986**, *870*, 545−551.

(20) Simpkin, D.; Ingledew, W. J. *Biochem. Soc. Trans.* **1984**, *12*, 500−501.

(21) Simpkin, D.; Ingledew, W. J. *Biochem. Soc. Trans.* **1985**, *13*, 603−607.

(22) Werth, M. T.; Cecchini, G.; Manodori, A.; Ackrell, B. A. C.; Schröder, I.; Gunsalus, R. P.; Johnson, M. K. *Proc. Natl. Acad. Sci. U.S.A.* **1990**, *87*, 8965−8969.

(23) Kowal, A. T.; Werth, M. T.; Manodori, A.; Cecchini, G.; Schröder, I.; Gunsalus, R. P.; Johnson, M. K. *Biochemistry* **1995**, *34*, 12284−12293.

(24) Wagner, G. C.; Kassner, R. J.; Kamen, M. D. *Proc. Natl. Acad. Sci. U.S.A.* **1974**, *71*, 253−256.

(25) Holländer, R. *FEBS Lett.* **1976**, *72*, 98−100.

(26) Clark, W. M. *Oxidation−Reduction Potentials of Organic Systems*; Baillière, Tindall & Cox Ltd.: London, 1960; pp 125 and 507.

(27) Cammack, R.; Crowe, B. A.; Cook, N. B. *Biochem. Soc. Trans.* **1986**, *14*, 1207−1208. Cammack, R.; Maguire, J. J.; Ackrell, B. A. C. In *Cytochrome Systems: Molecular Biology and Bioenergetics* IUB Symp. No. 159, 1988.

(28) Salerno, J. C. *Biochem. Soc. Trans.* **1991**, *19*, 599−605.

(29) Robinson, J. J.; Weiner, J. H. *Can. J. Biochem.* **1982**, *60*, 811−816.

(30) Cammack, R.; Chapman, A.; McCracken, J.; Cornelius, J. B.; Peisach, J.; Weiner, J. H. *Biochim. Biophys. Acta* **1988**, *956*, 307−312.

lent noncatalytic and catalytic voltammetry, with peak-like signals that are obtained in the absence of substrate transforming into steady-state catalytic waves upon addition of fumarate. The kinetic constants measured at pH 7.0 and 25 °C compared very well with data reported for conventional steady-state studies. As we now describe, the voltammetric features respond in well-defined ways to changes in pH and electrode rotation rate, and FrdAB thus provides an excellent model system for developing voltammetric methods to study intramolecular electron transfer in complex enzymes.

## Experimental Section

The soluble FrdAB domain was isolated from *E. coli* HB101/pFrd117 by an established method[30] and stored as ammonium sulfate pellets in liquid nitrogen. The specific activity for oxidation of reduced benzylviologen by fumarate was 392 units/mg at pH 6.8. Due to the oxygen sensitivity of the soluble enzyme, all experiments and preliminary handling were undertaken in a glovebox (Vacuum Atmospheres) under a nitrogen atmosphere (oxygen < 2 ppm). All solutions were made up with purified water (Millipore: 18 MΩ/cm). Prior to experiments, ammonium sulfate and other salts present in the samples were removed by diafiltration (Amicon 8MC fitted with a YM10 membrane) against 5 mM HEPES (*N*-[2-hydroxyethyl]piperazine-*N*′-[2-ethanesulfonic acid]) buffer at pH 7.5.

The thermostated electrochemical cell[10] was housed in a Faraday cage. A pyrolytic graphite edge (PGE) rotating disc electrode (geometrical area 0.03 cm$^2$ [31] ) was used in conjunction with an EG&G M636 electrode rotator, a platinum wire was used as counter electrode, and a saturated calomel electrode (SCE) in a Luggin side arm containing 0.1 M NaCl was used as reference. Voltammetry was performed with an Autolab electrochemical analyzer (Eco Chemie, Utrecht, The Netherlands) controlled by GPES software and equipped with an analogue Scan Generator and an Electrochemical Detection (increased sensitivity) module. All potentials are reported with reference to the standard hydrogen electrode (SHE), based on a potential of 242 mV for SCE at 20 °C.[32]

Experiments were performed with a mixed buffer system consisting of sodium acetate, MES (2-[*N*-morpholino]ethanesulfonic acid), PIPES (1,4-piperazinediethanesulfonic acid), HEPES, and TAPS (*N*-tris-[hydroxymethyl]methyl-3-aminopropanesulfonic acid), all purchased from Sigma, with final concentrations of 50 mM each and containing 0.1 M NaCl as additional supporting electrolyte. Mixtures were titrated with NaOH or HCl to the desired pH at 20 or 2 °C. To promote and stabilize the protein film, polymyxin B sulfate (Sigma) was added from a stock solution (10 g/L) with the pH adjusted to approximately 6, 7, or 8. The pH of final solutions was always checked at the experimental temperature. Aliquots of FrdAB were added from the diafiltered solution, and final cell concentrations (typically 1 $\mu$M) were estimated from the amount of enzyme in the pellet and subsequent dilution factors. Fumaric acid (Fluka, 99.5%) was added from freshly prepared stock solutions (1 or 10 mM) neutralized with NaOH. Oxalacetate inhibition studies were carried out with chloride-free buffers, made either by titrating 0.10 M sodium HEPES to pH 7.0 with 0.10 M MES (acid form) or 0.1 M PIPES (acid) with NaOH, in order to avoid interference by $Cl^-$ ions.[33,34] Fresh stock solutions of oxalacetate (Fluka, 99%) were used within 2 h.

For each experiment, the PGE electrode was polished with an aqueous alumina slurry (Buehler, 1 mm) and sonicated thoroughly. The enzyme was adsorbed on the surface by holding the potential at −160 mV (SHE) for 2 to 5 min. A freshly-treated electrode was used for each experiment. Temperatures were chosen to optimize either stability/coverage (2 °C) or activity (20 °C).

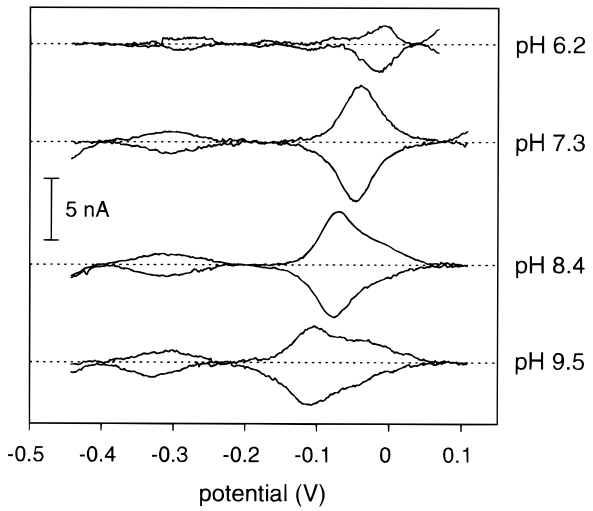


**Figure 1.** Voltammograms obtained for FrdAB at a PGE electrode (area 0.03 cm$^2$) in the absence of fumarate, corrected for non-faradaic background current. The scan rate is 10 mV s$^{-1}$ (analogue mode), and the temperature is 2 °C. The electrolyte consisted of 1.2 $\mu$M FrdAB in mixed buffer containing 0.2 g/L polymyxin and 0.10 M NaCl. The pH 6.2 data are the average of 4 scans, the pH 7.3 data are the average of 14 scans (3, 3, 3, and 5 scans with 4 different protein films), and the pH 8.4 and pH 9.5 data are both obtained by averaging two times 5 scans.

When necessary, the catalytic data were smoothed by using an in-house Fast-Fourier-Transform routine. The resulting curve was always checked for broadening of both the sigmoidal current and its peak-shaped first derivative d*i*/d*E*. The catalytic voltammograms were corrected for non-faradaic background current by subtracting a linear baseline from the derivative, *i.e.* by a second-order polynomial for the wave itself. The baseline was optimized visually, such that at low and high potential extremes, a range of at least 50 mV was observed where the corrected current was constant (and the derivative close to zero). For the noncatalytic data, the noise level was reduced by averaging of multiple scans rather than by smoothing. Deconvolution of the non-turnover peaks was performed by a least-squares fit to the sum of four voltammetric peaks (for Centers 1, 2, and 3 and FAD, using eq A.3) in addition to a fourth order polynomial baseline. For the one-electron centers, an ideal $n = 1$ peak was assumed; surface concentrations were equalized for all four centers.

## Results and Discussion

**Non-turnover Response at Slow Scan Rates.** In the absence of fumarate, adsorption of FrdAB gives rise to two reversible peak-like faradaic responses in the potential range 200 to −500 mV vs SHE.[10] The more prominent of these appears in the region close to that reported for the FAD while the smaller second signal occurs at much lower potential. As outlined previously and now developed below, these features identify enzyme centers participating in fast catalytic electron transport.

Figure 1 shows the baseline-subtracted faradaic components of slow-scan voltammograms measured at different pH values, and at a temperature of 2 °C to optimize coverage and stability. Structure is clearly discernible in the high-potential region. As shown in Figure 2, the observed "envelope" can be deconvoluted as the sum of a sharp two-electron peak ($n_{app} > 1$, see Appendix A) and two broader one-electron peaks. The reduction potential of the prominent peak with $n_{app} > 1$ decreases with a gradient of approximately 30 mV per pH unit and can be assigned to the FAD. At pH 7.3, the envelope is quite symmetrical, whereas at pH 9.5 a broad high-potential shoulder is clearly revealed. This comprises two one-electron signals, as expected for Centers

(31) The geometrical area of the electrode was determined to be 0.03 cm$^2$. This area did not significantly deviate from the electroactive surface area, determined from Levich plots (limiting current vs square root of rotation rate) for ferricyanide reduction as decribed in ref 10.

(32) Bard, A. J.; Faulkner, L. R. *Electrochemical Methods, Fundamentals and Applications*; Wiley: New York, 1980.

(33) Kearney, E. B.; Mayr, M.; Singer, T. P. *Biochem. Biophys. Res. Commun.* **1972**, *46*, 531−537. Kearney, E. B.; Ackrell, B. A. C.; Mayr, M.; Singer, T. P. *J. Biol. Chem.* **1974**, *249*, 2016−2020.

(34) Robinson, J. J.; Weiner, J. H. *Biochem. J.* **1981**, *199*, 473−477.

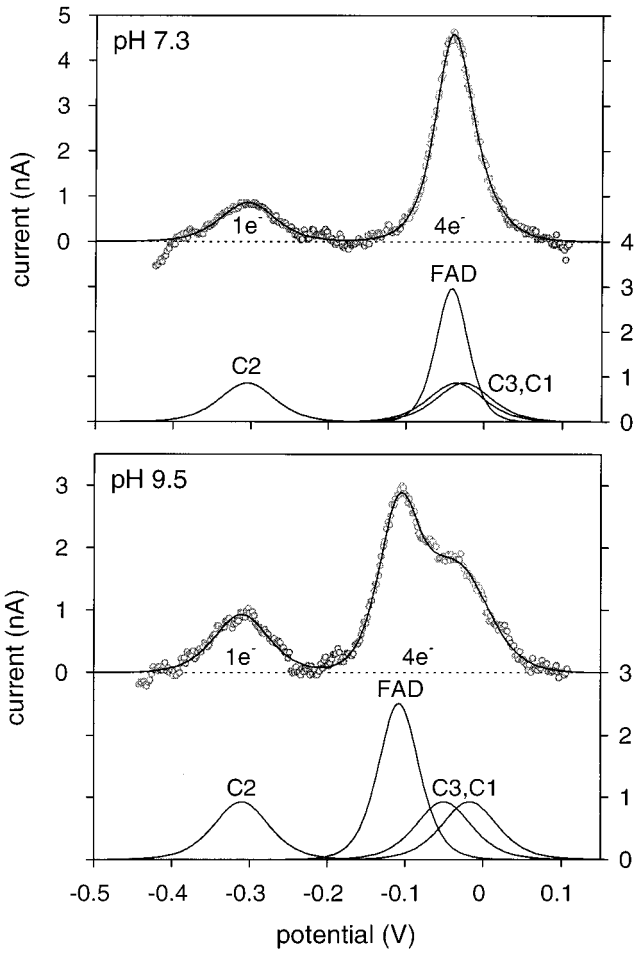


**Figure 2.** Deconvolution of the oxidation current, corrected for non-faradaic background current, at pH 7.3 and 9.5 (see Table 2 for parameters). Conditions as for Figure 1.

1 ([2Fe-2S]$^{2+/1+}$) and 3 ([3Fe-4S]$^{1+/0}$), which we assign in the order $E_1 > E_3$, based on the studies of Cammack and co-workers.[19] These authors explained the complex behavior of the EPR signals of Center 1 during redox titrations at pH 7 and 8.5 in terms of an intersite spin−spin interaction with $E_1 > E_3$. By contrast, the isolated weaker signal occurring at much more negative potential has the simple wave form expected for a reversible one-electron process: from its correspondence with published potentiometric data[16,19−23] this signal is assigned to Center 2 ([4Fe-4S]$^{2+/1+}$).

The results of the deconvolutions for pH 7.3, 8.4, and 9.5 are collated in Table 2 and are based upon the enzyme displaying a stoichiometry of 4 and 1 equivalents respectively in high- and low-potential regions. The deconvolutions yielded an average coverage ($\Gamma$) of 3.1 ± 0.3 pmol/cm$^2$, using the electrode area of 0.03 cm$^2$. Consequently, each FrdAB molecule effectively occupies an area of 5300 Å$^2$, equivalent to close-packed spheres of diameter 78 Å. This is similar to the value obtained earlier by a more approximate procedure and consistent with adsorption of an electroactive monolayer of molecules assuming spherical dimensions for a protein of 93 kDa (based upon a density of 0.8 g cm$^{-3}$).[35] Extrapolation of data to pH 7.0 yielded reduction potentials of −33 mV for FAD and −303 mV for Center 2, essentially identical with voltammetric values reported previously (−30 and −299 mV at 3 °C).[10] The *n* values measured for the FAD component appeared to decrease as the pH is raised (although this could also be due to greater inhomogeneity among protein molecules, which tends to disperse potentials and increase the width) but remained >1 in the oxidation direction, thus providing continued prominence within the envelope across the pH range studied.

The two-electron character of FAD transformations, more clearly evident at pH 7.3 and 8.4, was supported by the results of an EPR potentiometric titration.[36] A sample of FrdAB (36 $\mu$M) at 21 °C, pH 7.1, was titrated with sodium dithionite and equilibrated, using a cocktail of mediators, with a Pt electrode at potentials in the range +132 to −226 mV. No significant radical signals were observed at 165 K, and it was concluded that the maximum semiquinone level must be <2%.

**Non-turnover Response at Increased Scan Rates.** Voltammograms were measured at higher scan rates to examine the response of the prominent FAD component, and ascertain the expectation that redox transformations of this center involve intramolecular relay by Centers 1 and 3. Experiments were carried out at pH 6.2, 7.3, 8.4, and 9.5, and as before, at a temperature of 2 °C, where film coverage is improved. The scan rate was varied up to 20 V s$^{-1}$, with cycles initiated from both the high- and low-potential limits. The signals broaden with increasing scan rate, but it was still easy to track the movements of the FAD peaks with reasonable precision (±10 mV) because the underlying signals are much broader and do not significantly influence its position. Figure 3 shows plots of peak position against log{scan rate}. At pH 7.3, oxidation and reduction peak potentials separate symmetrically with scan rate, producing a "trumpet plot" with the simple shape expected for direct ET[37] or mediation by a relay system having well-matched potentials. By contrast, at pH 9.5, the oxidation peak is much more sensitive to scan rate, shifting markedly to higher potential and remaining more pronounced than the almost stationary reduction peak (which broadens and diminishes more rapidly; see above and Table 2). As outlined later, these results support an intramolecular ET mechanism in which FAD reduction and oxidation depend on a relay provided by Centers 1 and/or 3. The two-electron reduction potential of the FAD is matched closely to these Fe/S clusters at pH values around 7, but becomes relatively negative at pH 9.5. Thus at more alkaline pH, the energetics driving ET down the relay become increasingly biased *against* FAD reduction. The low-potential peaks assigned to Center 2 remained visible under all conditions examined and showed only a small increase in separation with scan rate, suggesting that interfacial ET is very facile and uncomplicated by coupling to other reactions.

**Appearance of the Catalytic Wave Form.** Addition of fumarate, with the electrode rotating at 200 rpm and higher, results in the high-potential envelope being replaced completely by a sigmoidal-like catalytic wave. As before, the absence of any residual peak-like features in the region of 0 to −100 mV indicates that all of the enzyme that is electroactive is also catalytically active.[10] To focus on the enzyme characteristics, it is necessary to remove or at least minimize rate limitations due to mass transport. We previously determined the enzyme kinetic parameters at pH 7, 25 °C, using Koutecky−Levich analysis to derive limiting current values at infinite rotation rate.[10] We noted that the catalytic wave distorts at high fumarate concentrations, and detected the emergence of a second sig-

(35) The high molecular mass of the protein obviously results in small peak currents (about 1 nA at 10 mV s$^{-1}$ for an $n = 1$ peak at full monolayer coverage) above a large non-Faradaic background (typically the difference between cathodic and anodic background is 150 times the height of an $n = 1$ peak with $\Gamma = 3$ pmol cm$^{-2}$). Data at pH 6.2 are close to the detection limit, and although the peak can still be found, this is largely due to the prominent FAD component and information about the shape and area of the envelope are lost. Cooperativity ($n > 1$) is a very valuable asset for detecting active sites since the peak current effectively varies as $n^2$ (see Appendix A).

(36) Dutton, P. L. *Meth. Enzymol.* **1978**, *54*, 411.

(37) Chidsey, C. E. D. *Science* **1991**, *251*, 919−922.

**Table 2.** Deconvolution of the Noncatalytic Peaks at 2 °C[a]

| | | $E_1$,[b] mV | $E_2$, mV | $E_3$,[b] mV | $E_{FAD}$, mV | $n_{FAD}$ | Γ, pmol cm$^{-2}$ |
|---|---|---|---|---|---|---|---|
| pH 7.3 | reduction | −31 | −304 | −66 | −47 | 1.8 | 2.9 |
| | oxidation | −26 | −305 | −36 | −41 | 1.7 | 2.8 |
| | average[c] | −28 (5) | −305 (−1) | −51 (30) | −44 (6) | | |
| pH 8.4 | reduction | −22 | −312 | −86 | −77 | 1.6 | 3.2 |
| | oxidation | −15 | −308 | −40 | −74 | 1.7 | 3.3 |
| | average[c] | −19 (7) | −310 (4) | −63 (46) | −76 (3) | | |
| pH 9.5 | reduction | −40 | −329 | −110 | −112 | 1.0 | 3.5 |
| | oxidation | −17 | −311 | −50 | −108 | 1.4 | 3.0 |
| | average[c] | −29 (23) | −320 (18) | −80 (60) | −110 (4) | | |

[a] The $n$ values for Centers 1, 2, and 3 are fixed at 1.0, and the surface coverage is equal for all four centers. Estimated error margins: $E_1$ and $E_3$ ±10 mV, $E_2$ ±5 mV, $E_{FAD}$ ±3 mV, $n_{FAD}$ ±0.2, and Γ ±0.3. [b] The assignment of the peaks is based on $E_{RED} \leq E_{OX}$ and $E_3 \leq E_1$ (ref 19). [c] Reduction potential; the peak separation $E_{pa} - E_{pc}$ is given in parentheses.

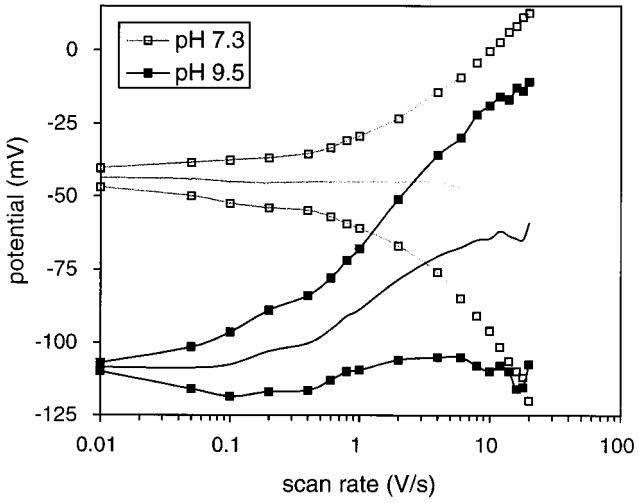


**Figure 3.** Scan rate dependence of the prominent high potential (FAD) peak positions at pH 7.3 and pH 9.5 at 2 °C. Cyclic voltammograms (analogue mode) were recorded starting at +0.24 V vs SHE, after 10 s of equilibration. The solution contained 1.0 μM FrdAB in mixed buffer containing 0.4 g/L polymyxin and 0.10 M NaCl.

moidal feature at a potential close to that of Center 2. This suggested that the [4Fe-4S] cluster provides a second relay system to mediate electrons to the FAD. Studies have now been carried out over the pH region 7−9, and with a wide range of fumarate concentrations and rotation rates. Since the aim was to obtain a useful semiquantitative picture of how the centers contribute to catalytic ET, a temperature of 20 °C was used to provide a good measurable level of activity over the entire pH range.

The waveforms are similar in each scan direction and independent of scan rate up to at least 50 mV s$^{-1}$, thereby showing that catalysis operates under steady-state conditions. Major changes in the waveform are observed as the pH is increased: overall, catalytic currents decrease significantly with respect to coverage and become much less dependent on rotation rate, while at the same time the second sigmoidal wave grows to provide a significant contribution to the rate. Representative results are shown in Figure 4. At pH 7.0, the second wave becomes clearly visible at 0.2 mM fumarate and high rotation rate (3000 rpm) and we estimate from extrapolation of data (to high fumarate concentration and infinite rotation rate) that it provides a maximum contribution of approximately 15% of the total catalytic current once mass transport limitation is removed. At increased pH, the waveform and current become independent of rotation rate, and the second wave contributes to a greater extent. Thus for pH 9.0, at which the activity for 0.2 mM fumarate is 20 times lower compared to pH 7.0,[38] the contribution of the second wave is 22%. At the highest tested pH of

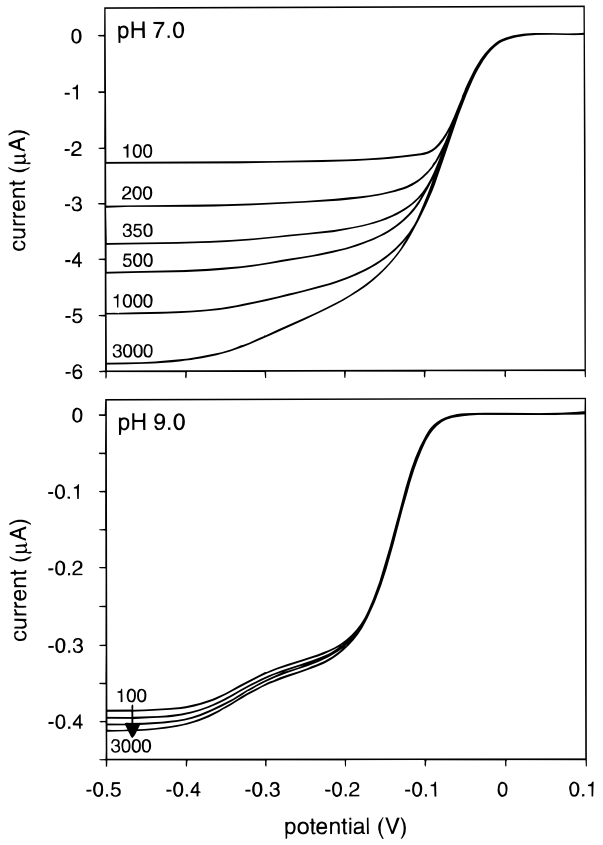


**Figure 4.** Rotation rate dependence of catalytic currents at pH 7.0 (100, 200, 350, 500, 1000, and 3000 rpm) and pH 9.0 (100, 200, 500, and 3000 rpm). The traces shown are the first reductive scans on fresh films for each rotation rate, corrected for the non-faradaic backgrounds and adjusted to equal coverage by using, as reference, a short excursion to 3000 rpm at low potential during the second scan. The scan rate is 10 mV s$^{-1}$ (staircase mode: fractional step time at which the current measured $\alpha = 0.5$ and step height $\Delta E = 2$ mV). The solution contained 0.9 μM FrdAB, 0.2 g/L polymyxin, 0.2 mM fumarate, and 0.10 M NaCl in mixed buffer at 20 °C.

9.5 and fumarate concentration of 0.8 mM (not shown) the contribution was 27%. The normalized wave forms (and relative amplitudes of each wave) were unchanged from one film to another or after prolonged periods of time, thereby showing the electrocatalytic response to be "binary", i.e. degraded enzyme effectively makes zero contribution.

(38) Although we have not undertaken a full kinetic study to obtain $k_{cat}$ and $K_M$ at pH 9, it is clear that $K_M$ for fumarate is much higher, since the catalytic currents continue to increase as the substrate concentration is raised above 1 mM (cf. pH 7, at which $K_M = 0.16$ mM at 25 °C). Weaker binding of dicarboxylates at increased pH is expected if residues in the active site undergo deprotonation.

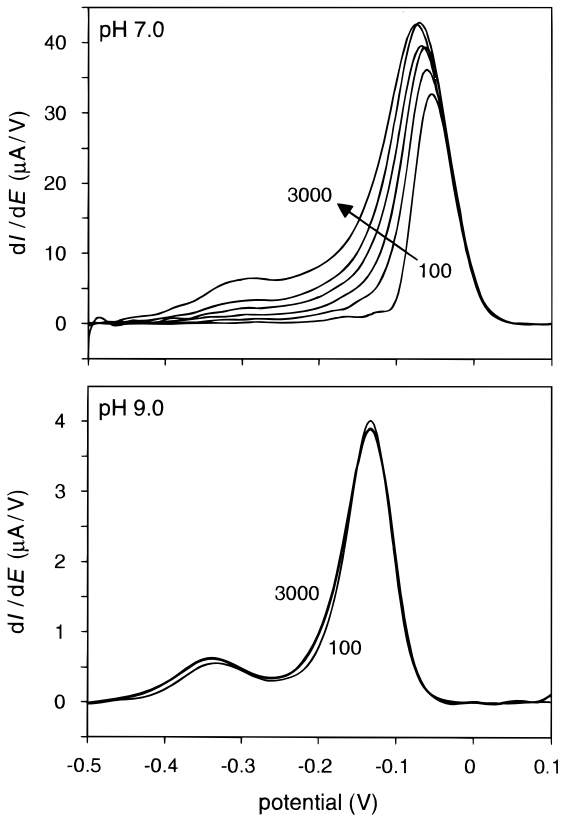


**Figure 5.** Derivatives (d*i*/d*E*) of the traces shown in Figure 4. For pH 9.0 only the traces at 3000 (thick line) and 100 rpm (thin line) are shown.

Figure 5 shows first derivatives (d*i*/d*E*) of the catalytic current with respect to potential. The transformation from waves to peaks facilitates wave form analysis and provides greater sensitivity to detect irregularities in catalytic ET. Most obviously, subtle alterations in turnover rate vs potential may occur as different centers begin (or cease) to participate in a relay, or modify activity by acting as redox-sensitive switches. The half-height peak widths give *n* values for the catalytic electron transport processes. Fumarate is an obligatory two-electron oxidant, and so for 100% mass-transport control we expect $n = 2$; necessarily only one such peak will be observed since an increase in rate cannot be induced by a higher driving force. By contrast, enzyme catalytic control will yield *n* values reflecting the properties of rate-determining steps and more than one peak may be observed if multiple relays contribute or if redox-sensitive regulatory centers alter the enzyme activity.[8,9,39]

For the pH 9.0 data, the derivative gives two clearly separated symmetrical peaks with half-height widths (see Appendix B) corresponding to *n* values of 1.4 and 1.0, respectively. Their form and peak positions are almost independent of rotation rate, and thus not mass-transport controlled. The potentials (ca. −140 and −330 mV) are close to the respective values observed for the FAD and Center 2 at pH 9.5 and 2 °C (see Table 2). By contrast, at pH 7.0, increasing the rotation rate produces major effects. At the lowest rotation rate shown (100 rpm), a single narrow peak is observed, corresponding to "$n = 1.5$". There is slight asymmetry, the wave being more abrupt on the low-potential side; this may be an artifact due to substrate depletion (i.e., electrode not rotating fast enough to replenish the diffusion layer) or may be due to mixed control by electron relay and mass transfer kinetics.[39] As the rotation rate is raised, the peak potential decreases, the peak broadens, and the low-potential peak begins to appear at −310 mV. At 3000 rpm, the *n*-value of the high-potential peak has decreased to 0.8, and there is some "tailing". Under all conditions, the low-potential peak remains close to $n = 1.0$.

**Oxidation-State-Dependent Oxalacetate Binding and Inhibition.** So far, we have described the catalytic ET profile observed under steady-state conditions. Oxalacetate (OAA) inhibits fumarate reductase, binding close to the FAD and more tightly to the oxidized form.[18] Thus, with OAA at levels lying between the dissociation constants for oxidized and reduced forms, fumarate reductase can be activated by reduction, and inactivated by oxidation during the course of a single cyclic voltammogram. This type of experiment was reported recently for succinate dehydrogenase, where activation and inactivation were observed to be slow.[8] It now provided an excellent way to perturb the FrdAB catalytic steady state, enabling intramolecular ET processes to be studied in transient mode.

First, oxalacetate binding to adsorbed FrdAB was measured voltammetrically in the absence of fumarate, by monitoring the position of the FAD component. Rates of binding and release were slow and it was necessary to scan at a very slow rate (1 mV $s^{-1}$) to achieve equilibration among species. As expected, oxalacetate decreases the reduction potential, consistent with stronger binding to the oxidized form. A sigmoidal plot of reduction (peak) potential against log(OAA) was obtained from which dissociation constants $K^{ox}$ and $K^{red}$ were estimated by fitting the data to eq 2.

$$E_{app} = E^{0\prime} + \frac{RT}{2F}\ln\left(\frac{1 + [\mathrm{OAA}]/K^{red}}{1 + [\mathrm{OAA}]/K^{ox}}\right) \qquad (2)$$

Equation 2 follows from a four-species square scheme for reversible two-electron reduction of the FAD with reversible oxalacetate binding to both the oxidized and reduced states.[40] Results for two temperatures, 2 (pH 7.0) and 20 °C (pH 6.9), are shown in Figure 6. We obtained $K^{ox} = 1.9$ $\mu$M and $K^{red} = 66$ $\mu$M at 2 °C and $K^{ox} = 0.07$ $\mu$M and $K^{red} = 205$ $\mu$M at 20 °C. These differ slightly, although not significantly, from the published values determined by non-electrochemical competition experiments.[18] Addition of $Cl^-$ resulted in weaker binding, showing that it interferes in a similar way to $Br^-$, as reported previously.[33,34]

A remarkable voltammetric response is observed when fumarate is added to the solution containing an intermediate level of oxalacetate. Experiments were run in the absence of $Cl^-$. Instead of the normal catalytic wave, hysteresis is observed, with reductive and oxidative scans respectively revealing activation and deactivation processes that switch abruptly at specific potentials. Figure 7 shows the results obtained at 2 °C. Similar behavior was observed at 20 °C, except that the faster rates of activation and deactivation produced voltammograms with a different shape. First, on commencing from a 2-min poise at +0.24 V, the catalytic current increases slowly below a threshold of −30 mV, i.e. in the high-potential envelope, then more steeply below −300 mV, i.e. at the reduction potential of Center 2. By contrast, the shape of the reverse (oxidative) scan resembles that observed in the absence of oxalacetate. The second cycle is similar except that residual activity is still apparent below −30 mV in the reductive scan. This residual activity could be quenched by holding the potential at the positive limit for a short period before recommencing.

(39) A manuscript presenting detailed analysis and modeling of the catalytic wave shapes and their interpretation is currently in preparation.

(40) Gutman, M.; Bonomi, F.; Pagani, S.; Cerletti, P.; Kroneck, P. *Biochim. Biophys. Acta* **1980**, *591*, 400−408.

(41) Cecchini, G.; Sices, H.; Schröder, I.; Gunsalus, R. P. *J. Bacteriol.* **1995**, *177*, 4587−4592.

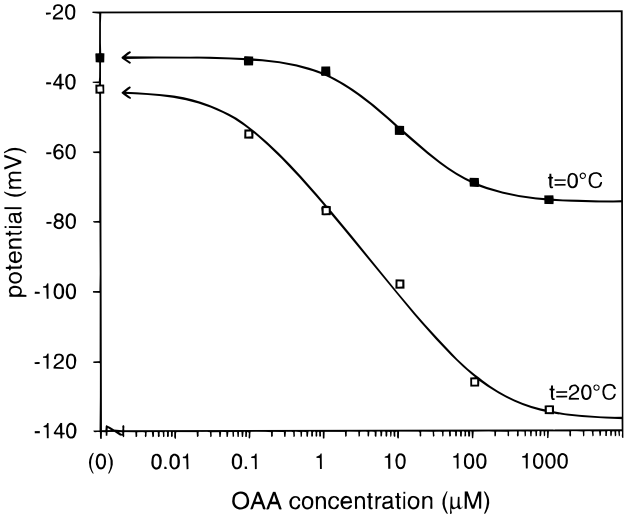


**Figure 6.** Positions of the FAD oxidation peaks in the presence of oxalacetate. The solution contained 0.9 $\mu$M FrdAB and 0.2 g/L polymyxin in 0.10 M chloride-free PIPES/NaOH buffer at pH 7.0 (2 °C) and pH 6.9 (20 °C). Voltammograms were recorded at 1 mV $s^{-1}$ (analogue mode). The lines show fitted traces for oxalacetate binding to a 2-electron center with $E_p^0 = -33$ mV, $K_D^{ox} = 1.9$ $\mu$M, $K_D^{red} = 66$ $\mu$M at 0 °C and $E_p^0 = -43$ mV, $K_D^{ox} = 0.069$ $\mu$M, $K_D^{red} = 205$ $\mu$M at 20 °C.

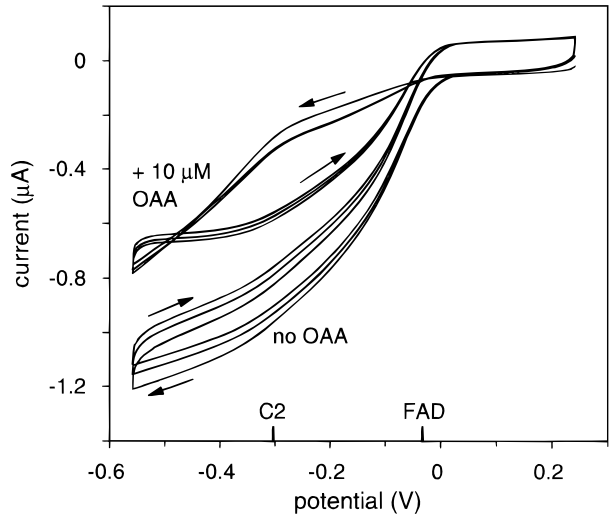


**Figure 7.** Catalytic voltammograms of FrdAB with and without oxalacetate. Shown are the first three cycles, recorded at 10 mV $s^{-1}$ (analogue mode) after 120 s of equilibration at +0.24 V vs SHE, rotation rate 1000 rpm at 2 °C. The solution contained 1.2 $\mu$M FrdAB, 0.2 g/L polymyxin, and 0.10 mM fumarate in 0.10 M chloride-free HEPES(Na)/MES(H) buffer at pH 7.0. The potentials of the FAD (−33 mV) and Center 2 (−303 mV) from Table 1 are indicated on the horizontal axis.

The activation kinetics were investigated by chronoamperometry in the presence of fumarate. This technique enables the current (catalytic rate) to be measured directly in the time domain—initiation or de/activation of the catalytic reaction being executed by "jumping" the potential between different values.[32] Potential steps were made across the range −200 to −400 mV, each preceded by a 30-s period at +0.24 V to oxidize the active site and allow rebinding of oxalacetate. Because oxalacetate dissociation is slow, the observed current at any time will be proportional to the fraction of active enzyme. In each case, the rate of current increase followed a single exponential. As shown in Figure 8, the activation rate constants are potential dependent, increasing sigmoidally from 7.8 × $10^{-3}$ $s^{-1}$ (half life 88 s) at −200 mV, to 0.052 $s^{-1}$ (half life 13 seconds) at −400 mV, the "half-wave" potential being −284 mV.

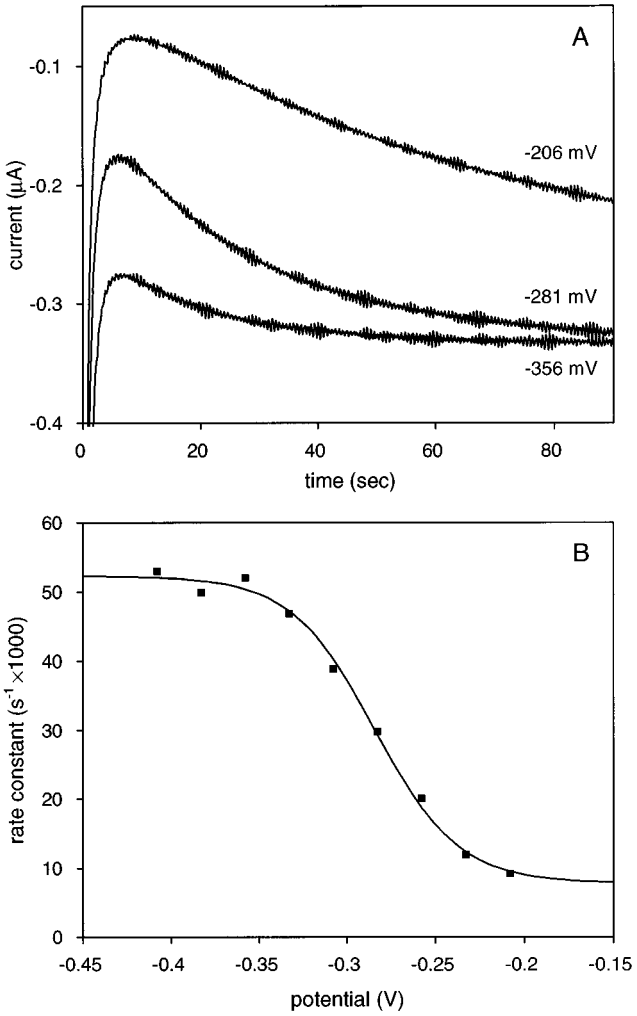


**Figure 8.** (A) Chronoamperometric traces at different applied potentials, showing the increasing (negative) catalytic current in addition to the decaying interfacial charging current. Each measurement was preceded by 30 s of equilibration at +0.24 V. The solution contained 1.1 $\mu$M FrdAB, 0.2 g/L polymyxin, 0.1 mM fumarate, and 10 $\mu$M oxalacetate in 0.10 M chloride-free HEPES(Na)/MES(H) buffer at pH 7.0 and 2 °C. Note the increasing activation rate as the potential is lowered. (B) First-order rate constants for reductive activation. The line shows a fit of the data (average of four runs on two protein films) to a sigmoidal wave with limits of 7.8 × $10^{-3}$ and 5.2 × $10^{-2}$ $s^{-1}$ and a halfwave potential of −284 mV.

## General Discussion

Recent reports from this laboratory have described how voltammetry can be applied to detect and study subtle features of enzyme catalytic ET including cooperativity, redox-dependent regulation, catalytic bias, and H/D isotope energetics.[4,6−10] The results presented in this work provide further illustrations of how voltammetry can be used to probe complex ET enzymes. The key features are as follows: (a) that electron exchange between electrode and one or more relay stations in the enzyme is effectively reversible, thus ensuring that electrode kinetics are not a limiting factor, (b) that catalytic activity is retained, with substrates having a high level of accessibility to the enzyme's catalytic site, (c) that the coverage of active enzyme is sufficiently high to observe signals in the absence of catalytic turnover, and (d) that these molecules behave homogeneously and in a binary manner, i.e. that degraded or poorly oriented

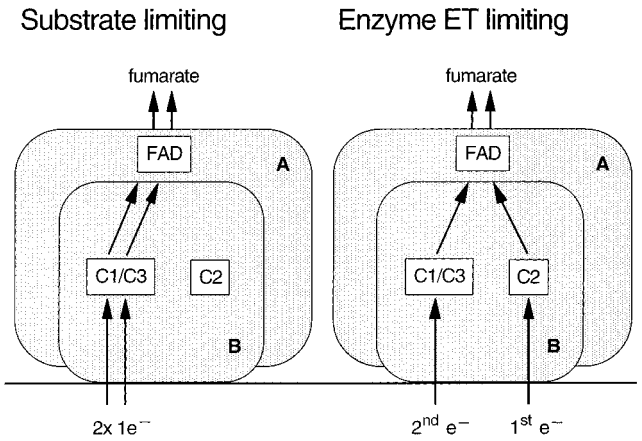


**Figure 9.** Schematic representation of the proposed electron relay model. When substrate mass transport is the limiting factor, both electrons are provided via Centers 1 and 3. If enzyme ET is rate limiting, Center 2 assists by relaying electrons at low potential.

enzyme is completely inactive and does not therefore corrupt the voltammogram. Note that a heterogeneous population of *active* molecules would cause dispersion of potentials (broadening of noncatalytic signals) and very likely some variation in catalytic constants from one experiment to another (which would be clearly evident as differences in shape among normalized catalytic waves).

At pH 7, and in the absence of fumarate, well-behaved two-electron transformations of FAD are observed in both oxidative and reductive directions up to 20 V $s^{-1}$. The symmetrical plot shown in Figure 3 is as would be expected if FAD was oxidized and reduced directly, i.e. without participation of a relay. However, that this simple but unlikely explanation is *not* the case is revealed by the experiments at higher pH, where the FAD reduction and oxidation peaks display increasing distortion and displacement to higher potential (the region of Centers 1 and 3). Very similar results were obtained irrespective of whether the scan was commenced at high or low potential limits, indicating that the observed shift is not due to gating by a coupled slow chemical reaction. Thus as the scan rate is increased, fewer electrons pass through to the FAD under reducing conditions, while oxidation of FAD occurs rapidly but at a significantly higher potential. This type of behavior is predicted if electrons are relayed to FAD by Centers 1 and 3, since the FAD becomes a poorer acceptor (but a better donor) as the pH is raised.

The results observed for FrdAB are most readily interpreted in terms of intramolecular electron transfer involving two relay systems, one with a small driving force involving Centers 1 and 3, the other at a more negative potential involving Center 2. As discussed later, these relays each have the character of separate one-electron rather than cooperative two-electron transfers. As an aid for reference, the working model is displayed in Figure 9, and arrows indicate the relative importance of each relay. Independent evidence that the high-potential relay comprises both Centers 1 and 3 stems from several sources. Mutations of the intact enzyme (FrdABCD) which lower the potential of either of these clusters result in serious retardation of the rate of reduction of fumarate by menaquinone.[16,22] In addition, there is evidence that the [3Fe-4S] cluster is the first relay station for electron exchange with quinones.[41] The FrdAB catalytic unit does not interact with quinones, but it is certain from the voltammetry that at least one of these clusters provides a relay from the electrode. Correlating all the voltammetric data, there can be little doubt about the involvement of Center 2 in catalytic ET. The first and most obvious proposal is that Center 2 operates directly as a relay, delivering one of the electrons for catalysis. An alternative proposal for the second wave invokes communication between Center 2 and other sites, so that the catalytic rate constant for ET occurring via Centers 1 and 3 depends on whether Center 2 is oxidized or reduced. This cannot be ruled out, but seems unlikely since the non-turnover signal assigned to Center 2 behaves as expected for a fast, uncomplicated redox couple.

Center 2 makes its greatest contribution at higher pH and elevated fumarate levels. There are two reasons for this. First is the more trivial point that rate-determining processes in the enzyme are masked under conditions of mass-transport control. Thus if the enzyme is very active, i.e. as at pH 7, the second sigmoid becomes evident only at high fumarate concentration and high electrode rotation rate which optimize substrate supply and relieve mass-transport control. By contrast, FrdAB is much less active at pH 9, as shown by the smaller catalytic currents (Figure 4) despite similar coverage (Figure 1).[38] Substrate levels in the vicinity of the enzyme are not depleted (the voltammetry is virtually insensitive to rotation rate), and catalytic ET comes automatically under enzyme control—the condition required for detecting effects that are characteristic of the enzyme.[10] Enzyme-controlled electrocatalysis is similarly observed[8,9] for succinate dehydrogenase, enabling deconvolution of its otherwise complex voltammmetry. The second reason concerns the true intrinsic contribution of the Center 2 relay, which at alkaline pH becomes relatively more important since Centers 1 and 3 function less effectively as donors to the more reducing FAD. The question remains as to the physiological role of Center 2, as discussed by several authors. The 3D structure of fumarate reductase has yet to be solved, so the exact relative locations of the redox sites are not known. Whatever the outcome, however, our experiments on the catalytic AB domain now show conclusively that Center 2 contributes significantly to the catalytic ET activity. Although participation requires potentials that are negative compared to *stable* forms of known reaction partners in the respiratory chain, the possibility remains that the two menaquinone molecules that are bound tightly to FrdC and FrdD subunits may shuttle electrons via more reducing radical states.[15,42]

The utility of Center 2 is manifested further in the reductive activation of oxalacetate-inhibited enzyme, where its engagement immediately provides a 7-fold increase in activation rate. Oxalacetate-bound FrdAB is totally inactive, so a catalytic current is observed only once the inhibitor is released. Reductive activation of oxaloacetate-bound FAD is also observed for succinate dehydrogenase,[8] where (as with FrdAB) the kinetics are slow, most likely because some rearrangement is required.[12,18] At the oxalacetate concentration used (10 $\mu$M), the inhibitor is bound if FAD is oxidized ($K^{ox}$ = 1.9 $\mu$M) but is released upon reduction ($K^{red}$ = 66 $\mu$M). Assuming that the rates of binding and release depend only on the oxidation state of the FAD, we can rationalize the chronoamperometric transients in terms of ET rates along two relays. The limiting values of the sigmoidal plot of activation rate against potential are (lower) $8 \times 10^{-3}$ $s^{-1}$ at −200 mV (Center 2 oxidized) and (upper) 0.052 $s^{-1}$ at −400 mV (Center 2 reduced). The lower limit (at −200 mV) thus corresponds to the rate of reduction of oxalacetate-bound FAD as relayed by using Centers 1 and 3. At first glance, the upper limit may be assumed to correspond to the rate of reduction by Center 2: however, the half-wave potential of the plot −284 mV is a little higher than actually

(42) Westenberg, D. J.; Gunsalus, R. P.; Ackrell, B. A. C; Sices, H.; Cecchini, G. *J. Biol. Chem.* **1993**, *268*, 815−822. Yankovskaya, V.; Sablin, S. O.; Ramsay, R. R.; Singer, T. P.; Ackrell, B. A. C.; Cecchini, G.; Miyoshi, H. *J. Biol. Chem.* **1996**, *271*, 21020−21024.

observed for Center 2 (−303 mV, which we note is unchanged by oxalacetate binding at 2 °C in the absence of fumarate). If the plot is reconstructed by using the lower (−200 mV) limiting rate but fixing $E_{1/2}$ at −303 mV, i.e. as expected for Center 2, the upper limit (at −400 mV) is increased approximately 2-fold. The most likely interpretation is that the *experimental* upper limit corresponds instead to the rate of release of oxalacetate from reduced FAD whereas the *extrapolated* rate gauged by the reconstructed curve (approximately 0.1 $s^{-1}$) corresponds to the rate of electron transfer from Center 2.

Interestingly, rates of intramolecular ET to the oxalacetate-bound FAD are orders of magnitude lower than during normal turnover (which must be at least equal to $k_{cat} = 875$ $s^{-1}$ at 25 °C, or 14 $s^{-1}$ at 3 °C[10]). Such a large retardation cannot be explained by the decrease in reduction potential of the FAD, since the maximum shift is just 42 mV at 2 °C (95 mV at 20 °C) compared to approximately 60 mV (30 mV per pH unit) when raising the pH to 9, which still results in viable ET. The special efficacy of Center 2 in reductive activation has several possible explanations. First, oxalacetate might further destabilize the semiquinone state, lowering the first reduction potential $E^{0\prime}{}_1$ very significantly so that Centers 1 and 3 become particularly ineffective donors. This is plausible since substrate binding increases the stability of the flavosemiquinone formed in succinate dehydrogenase,[43] but is difficult to test for FrdAB given (a) that the FAD semiquinone radical is barely detectable even in the free enzyme and (b) that the two-electron FAD voltammetric signal is already narrow and thus a rather insensitive indicator of further cooperativity. A second explanation is that oxalacetate binding increases the reorganization energy $\lambda$ (low rates if $\Delta E < 2\lambda$), rendering the low-potential donor much more effective. Other possibilities are that oxalacetate causes a conformational change which alters the pathway (electronic coupling) or (as hinted earlier) that Center 2 is a regulatory site. Obviously, these options remain speculative at the present time.

Finally, there is the capability, as yet virtually unexplored, for the detailed analysis of rate-determining steps. The catalytic voltammetry of FrdAB at PGE spans a wide range of behavior, being limited at the one extreme by mass transport or at the other by enzyme catalysis, with the interfacial electron transfers being effectively reversible throughout. The results give no indication that interfacial electron transfer is rate limiting. In principle therefore, we expect the *n* values of waves to correspond on the one hand (mass-transport control) to the overall stoichiometry of the catalyzed reaction and on the other hand (enzyme catalytic control) to reveal the number of electrons passing through the rate-determining catalytic step. Under the condition of steady-state mass-transport control, which is achieved for the rotating electrode at certain conditions (high enzyme activity with low fumarate concentration, low rotation rate), the *n* value of the single wave lies in the expected region of 2.0. Alternatively, at the limit of enzyme catalytic control (low enzyme activity, high fumarate concentration, high rotation rate) we invariably observe that the derivative plot stabilizes, giving peaks with *n*-values that approach 1.0. A notable similarity is found with the catalytic voltammetry of succinate dehydrogenase, which so far has appeared strictly enzyme controlled (no rotation rate dependence), and consistently yields $n = 1.0$ for succinate/fumarate interconversion over a wide range of conditions (although this is complicated by reversion to a less-active form when the FAD is reduced).[8] Significantly, the limiting *n* values observed for FrdAB catalytic voltammograms contrast with the much more obvious cooperativity shown by the FAD component under non-turnover conditions, and with the fact that fumarate is an obligatory two-electron acceptor. The identification of one-electron transfers as determinants of the course of catalytic ET now represents important mechanistic information that can be used to model the entire system.[39]

In conclusion, protein-film voltammetry provides a very different perspective on catalytic ET to that obtained from conventional kinetic studies. The results we have described illustrate further ways in which the method can be employed for the study of enzymes and biological electron transfer. We have discussed the correlation between noncatalytic and catalytic voltammograms and shown how ET is defined in terms of a potential/activity profile, effectively a "spectrum", in which readily measurable features—signals from centers and changes in ET rate—are identified at characteristic potentials. Thus, in a unique way, the experiments probe the "potential domain" in addition to the normal time domain. Information is gained on the electron-transfer processes (rates and cooperativity) occurring at certain characteristic energies, both under non-turnover conditions and during turnover, where even the subtlest irregularities may be revealed from the derivative voltammogram. So far, relatively few enzymes have proved amenable to study at electrodes: the information derived for fumarate reductase now serves as a good example of what is possible once the problems of stabilizing a protein film and achieving good interfacial electron transfer are overcome.

**Acknowledgment.** This work was supported by grants from the Wellcome Trust (No. 042109 to H.A.H. and F.A.A.) and the Medical Research Council of Canada (PG-11440 to J.H.W.). Samples of FrdAB were prepared by Gillian Shaw. We thank Professor Fred Hagen (Wageningen, The Netherlands) for use of EPR facilities. We also thank Dr. Artur Sucheta and Jim Whitehouse for making many of the early measurements in this work and Judy Hirst for helpful discussions.

## Appendix A: The Shape of Voltammetric Peaks

For a diffusionless, reversible (Nernstian) reaction involving concerted transfer of $n_s$ electrons

$$\mathrm{Ox} + n_s e^- \rightleftarrows \mathrm{Red}$$

with formal reduction potential $E^0$, the current can be derived as[32]

$$i = -n_s F A \frac{d\Gamma_{Red}}{dt} \tag{A.1}$$

and

$$\Gamma_{Red} = \frac{\Gamma_{total}}{1 + \exp\{n_{app}F(E - E^0)/RT\}} \tag{A.2}$$

yielding

$$i = \frac{n_s n_{app} F^2 \upsilon A \Gamma}{RT} \frac{\exp\{n_{app}F(E - E^0)/RT\}}{(1 + \exp\{n_{app}F(E - E^0)/RT\})^2} \tag{A.3}$$

where $\upsilon$ is the scan rate, $\Gamma$ is the surface concentration, $A$ is the electrode area, and $E$ is the applied potential. The other symbols have their usual meaning. This describes a peak-shaped current, symmetrical around $E^0$ and with a peak width at half height

$$\delta = 3.53\frac{RT}{n_{app}F} \tag{A.4}$$

(43) Bonomi, F.; Pagani, S.; Cerletti, P.; Giori, C. *J. Biochem.* **1983**, *134*, 439−445.

(44) Plichon, V.; Laviron, E. *J. Electroanal. Chem.* **1976**, *71*, 143−156.

For ideal systems $n_{app}$ is equal to $n_s$. Thus, because the peak current is effectively proportional to $n^2$, two-electron reactions are four times more detectable than one-electron reactions. However $n_{app}$ can differ from $n_s$ due to non-idealities (e.g., coupled reactions, electron-transfer kinetics, preferential adsorption of one of the redox states, lateral interactions or dispersion of the redox properties).

Consider the degree of cooperativity for a two-electron process. We include a one-electron state S

$$\mathrm{Ox} + \mathrm{e}^- \rightleftarrows \mathrm{S} \qquad \text{with formal reduction potential } E^0{}_1$$

$$\mathrm{S} + \mathrm{e}^- \rightleftarrows \mathrm{Red} \qquad \text{with formal reduction potential } E^0{}_2$$

Plichon and Laviron[44] derived the general formula describing the shape of the voltammetric response for the diffusionless, Nernstian system:

$$\Psi(E) = \frac{i(E)}{\upsilon\Gamma A\, F^2/RT} = \frac{\sqrt{\xi} + 4/\sqrt{K} + 1/\sqrt{\xi}}{(\sqrt{\xi} + \sqrt{K} + 1/\sqrt{\xi})^2}\sqrt{K} \qquad \text{(A.5)}$$

with a coproportionation constant

$$K = \exp\left\{\frac{F}{RT}(E^0{}_1 - E^0{}_2)\right\} \qquad \text{(A.6)}$$

and a potential function

$$\xi = \exp\left\{\frac{2F}{RT}(E - E^0)\right\} \qquad \text{(A.7)}$$

where $E^0 = (E^0{}_1 + E^0{}_2)/2$ is the two-electron reduction potential. This shows that the separate one-electron potentials and thus the degree of cooperativity of the two reduction steps can be derived from the shape and the position of the peak. The peak shape can be summarized conveniently by a single parameter, the peak width at half height, which can be easily derived from experimentally measured voltammograms. However, Plichon and Laviron[44] did not give the analytical solution for the peak width and apparent $n$ value that will be found when eq A.4 is used.

To obtain the relation between the peak width and the difference between the one-electron potentials, the equation

$$\Psi(E) = \Psi_p/2 = 1/(2 + \sqrt{K}) \qquad \text{(A.8)}$$

with $\psi_p = \psi$ at $E = E^0$, must be solved. After rearrangement,

$$\xi^2 - K\xi^{3/2} + (K - 4\sqrt{K} - 6)\xi - K\sqrt{\xi} + 1 = 0 \qquad \text{(A.9)}$$

can be obtained, for which the real roots

$$\sqrt{\xi} = \mathrm{A} \pm \sqrt{\mathrm{A}^2 - 1} \qquad \text{(A.10)}$$

with

$$\mathrm{A} = \{K + \sqrt{K^2 - 4K + 16\sqrt{K} + 32}\}/4 \qquad \text{(A.11)}$$

are found. From these solutions, the potentials can be derived at which the current equals half the maximum current. The difference between these two potentials, located on the positive and the negative flanks of the peak, is the desired peak width at half height ($\delta$):

$$\delta = \frac{RT}{F}\ln\left\{\frac{\mathrm{A} + \sqrt{\mathrm{A}^2 - 1}}{\mathrm{A} - \sqrt{\mathrm{A}^2 - 1}}\right\} = \frac{2RT}{F}\ln\{\mathrm{A} + \sqrt{\mathrm{A}^2 - 1}\} \qquad \text{(A.12)}$$

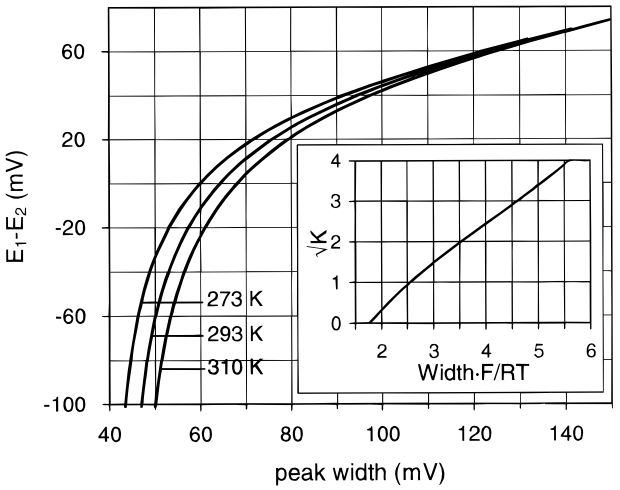


**Figure 10.** Working curve relating the peak width at half-height for a two-electron redox reaction and the difference between the two single-electron potentials. The inset is the generalized curve of the square root of the conproportionation constant versus the normalized peak width.

From this, a working curve is plotted (Figure 10) to obtain the comproportionation constant $K$ as a function of normalized peak width. The stability of the semireduced state S is given by the maximum relative concentration, occurring at $E = E^0$:

$$\frac{\Gamma_S}{\Gamma_{Ox} + \Gamma_S + \Gamma_{Red}} = \frac{\sqrt{K}}{2 + \sqrt{K}} \qquad \text{(A.13)}$$

and the apparent $n$ value for the two-electron redox reaction can be obtained (using $K = 0$ at $n = 2$, see below) from the peak width:

$$n_{app} = \frac{4RT\ln(1 + \sqrt{2})}{\delta F} \qquad \text{(A.14)}$$

When $K > 16$ two separate peaks are observed,[44] implying that the observation of a *single* peak that is broader than $5.60RT/F$ indicates that either the electron transfer is not purely Nernstian or that broadening of the peak has occurred due to dispersion of the redox properties. For an uncomplicated Nernstian reaction involving two electrons, several special cases can be found: When $K = 4$, $\delta = 4\ln(1 + \sqrt{2})RT/F \approx 3.53RT/F$, which means that the peak shape is exactly that of a one-electron reduction, but with twice the height. This implies that the cases of two independent one-electron processes with equal potentials and of a single two-electron process with $E^0{}_1 - E^0{}_2 = RT/2F\ln(4)$ (=18 mV at 25 °C) are indistinguishable. When $n_{app} > 1$ is found, the observed response must be assigned to a two-electron process with some degree of cooperativity. When the reduction potentials of the two steps are equal, $K = 1$ and $n_{app} = 1.38$. When $K = 0$, the potentials are infinitely "crossed", i.e. fully cooperative, with $\delta = 2\ln(1 + \sqrt{2})RT/F \approx 3.53RT/2F$. Assuming that the deviation must be at least 5% ($n < 1.9$, $K = 0.02$) to be detectable, $n_{app} = 2$ is found when the one-electron potentials are at least 100 mV "crossed" (at 25 °C).

## Appendix B: Analysis of Catalytic Wave Shapes

A symmetrical catalytic wave can be described by the Nernstian wave

$$i = \frac{i_{lim}}{1 + \exp\left\{\frac{nF}{RT}(E - E_{hw})\right\}} \qquad \text{(B.1)}$$

where $i_{lim}$ is the limiting (maximum) steady-state current for the catalytic wave (*i.e.*, the current at low potential) and $E_{hw}$ is the half-wave potential (the potential where the current is half of $i_{lim}$). The value of $n$ determines the steepness of the wave, and reflects the (apparent) number of electrons transferred in the catalytic reaction, or in the rate-limiting step. A higher value of $n$ results in a steeper wave, i.e., in a sigmoidal change from $i = 0$ to $i = i_{lim}$ that is more "compressed" around $E = E_{hw}$.

The classical way to analyze a wave of this type is to plot $\ln((i_{lim} - i)/i)$ *versus* $E$. This will give a straight line, crossing zero at $E = E_{hw}$ and a slope of $nF(E - E_{hw})/RT$. However, when the wave is not purely symmetrical, the log plot is not linear. And when multiple waves are present, $i_{lim}$ has to be determined for each wave separately. Alternatively, the wave can be analyzed by using its derivative $di/dE$. For a symmetrical wave, this yields a symmetrical peak around $E = E_{hw}$:

$$\frac{di}{dE} = -i_{lim}\frac{nF}{RT}\frac{\exp\left\{\frac{nF}{RT}(E - E_{hw})\right\}}{\left(1 + \exp\left\{\frac{nF}{RT}(E - E_{hw})\right)\right\}^2} \qquad \text{(B.2)}$$

With $n = 1$ or 2, the shape of this peak is exactly equal to that of a noncatalytic peak for a reversible one- or two-electron reaction (see Appendix A). The $n$ value (also when apparent, non-integer) can therefore be derived from the peak width at half height according to eq A.4.

JA9723242